

# Connections with inclined screws and increased shear plane friction

Simon Aurand, Hans Joachim Blass

Karlsruhe Institute of Technology (KIT), Timber Structures and Building Construction

Keywords: inclined screws, shear plane, friction, coefficient of friction COF

## 1 Introduction

Joist to header connectors are widely available in different shapes and sizes. One of the most common types resembles dovetail connections, where two parts slide into each other to enable load transfer (Figure 1a). Usually, aluminium is used for the connectors. One scope of the here presented project was to replace the aluminium with densified veneer wood (DVW). The connectors are mostly fastened with self-tapping and fully threaded screws, which are often inclined by  $45^\circ$  to the connector plane. In such connections with inclined screws, the load parallel to the shear plane is mainly transferred by axial screw loading, see *Bejtka & Blass (2002)*. Due to equilibrium conditions, a compressive force results perpendicular to the shear plane. This compressive force leads to frictional resistance, which depends on the size of the compressive force and the coefficient of friction  $\mu$ . For connections with inclined screws, this additional load-carrying capacity can be taken into account by default, although the screws are loaded in tension. This is the difference to connections under combined lateral and tensile load, where the load increase due to friction, i.e. the rope effect, cannot be applied. Another scope of the project was to utilize the frictional resistance, which depends on the size of the compressive force and the coefficient of friction (COF). Therefore, two possibilities can be examined: (i) increasing the compressive force by designing the connection to reach the tensile capacity of the screws and (ii) increasing the COF by treating the surface adequately. The latter was done in this study.

To increase the load-carrying capacity due to surface treatment, first an extensive literature review was accomplished. This was followed by own tests to modify the surface and determine the COF and hence the optimal modification. Following this, push-out tests with connectors made of the afore mentioned DVW were performed. Finally, an analytical model for the load-carrying capacity was derived.

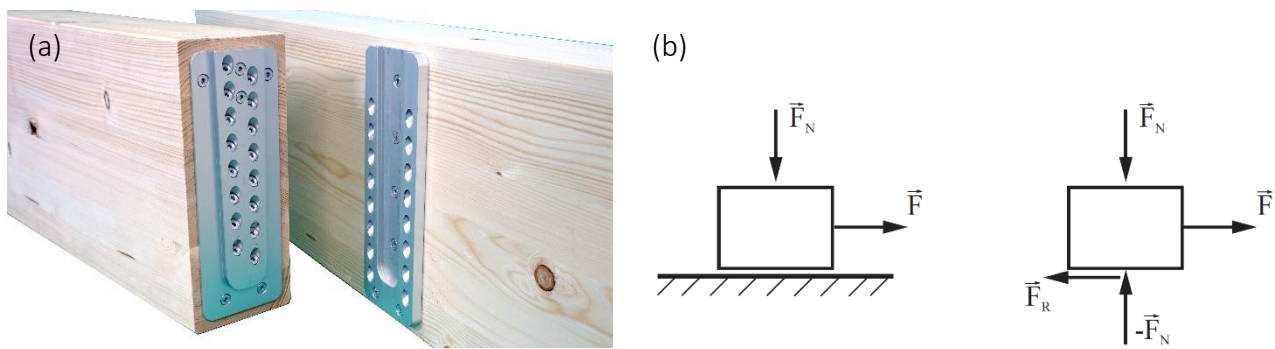


Figure 1. (a) Aluminium dove tail connector. (b) A body stressed by normal and tangential forces and the force equilibrium with the reaction force  $F_N$  and the friction force  $F_R$  (Popov (2015)).

## 2 Friction – Literature review

### 2.1 Introduction

The COF is defined as the dimensionless ratio of the friction force  $F_R$  between two bodies to the normal force  $F_N$  perpendicular to the contact area between these bodies (Figure 1b). The static COF  $\mu_{\text{stat}}$  corresponds to the maximum friction force that must be overcome to initiate relative displacement between two bodies.

In the literature, many different values for the static COF for wood on wood as well as steel on wood can be found. Table 1 gives an overview of the publications having determined the COF for wood on wood or wood on steel. Also given is the number of values, which were taken from the literature. This number is not necessarily equal to the performed tests. For example, *Stošić* (1959) performed 9000 tests in total, however, only ten values can be extracted from his two-page article. In most of the research listed in Table 1 many parameters were varied, such as the contact pressure between the specimens (normal force  $F_N$ ), the sliding speed, the surface roughness, the angle between the grain direction of the wood specimens and the sliding direction, as well as the moisture content. The following sections examine a possible correlation between the COF and the respective parameter.

The values in Table 1 and from Figure 3 through to Figure 9 are all taken from the literature and do not include test results from chapter 4.

### 2.2 Test setup

The most common test setups can be seen in Figure 2. Setup (a) with the inclined plane is very easy to use. The normal force is applied with weights and the plane is inclined just until the specimen starts sliding. However, due to the constantly changing contact pressure depending on the angle, the inclined plane is not suitable to determine the COF reliably (*Stošić* (1959)). Because of its simple design, the horizontal plane (b) was the most used test setup. This setup allows the evaluation of parameters such as contact pressure and sliding speed. Test setup (e) is similar to the horizontal plane with the only difference using a vertical cylinder to apply the normal force. The rotating plane in setup (c) was mostly used for tests with wood sliding on steel. An effective setup for higher contact pressure but without having to use a second cylinder is setup

(d) with pre-stressed rods. However, the size of the specimen is much larger than for the other tests and also the time to assemble the specimen takes longer. The last setup (f) for shear tests with inclined screws is not primarily used for determination of the COF, but the COF can be back calculated (*Blass & Steige (2018)*).

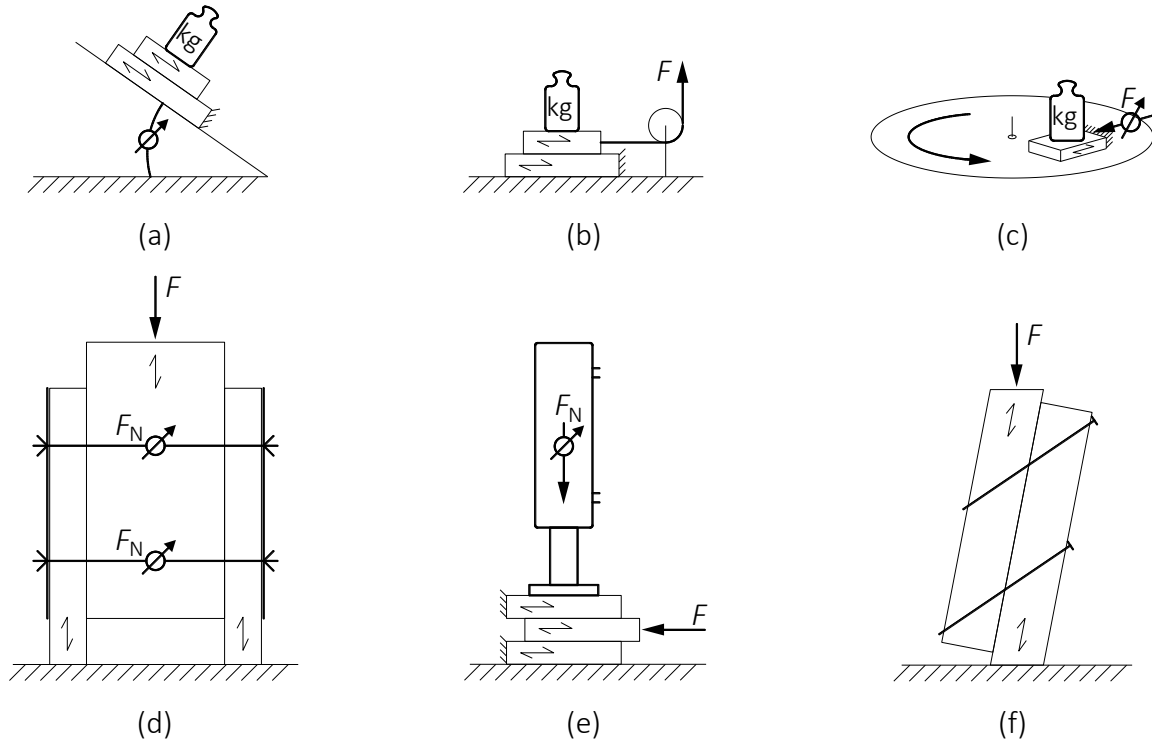


Figure 2. Test setups to determine the coefficient of friction: a) inclined plane b) horizontal plane, c) rotating plane d) pre-stressed rods e) two hydraulic cylinders f) shear tests with inclined screws.

### 2.3 Contact pressure

Figure 3 shows the influence of the contact pressure on the static COF. The recorded pressures ranged from 0.0001-1.0 N/mm<sup>2</sup> for tests with wood on wood and from 0.0069-30 N/mm<sup>2</sup> for tests with steel or aluminium on wood. The logarithmic trend line shows firstly an increase of the COF with rising contact pressure and later a horizontal convergence. For the tests with steel / aluminium on wood, no correlation between the COF and the contact pressure can be observed.

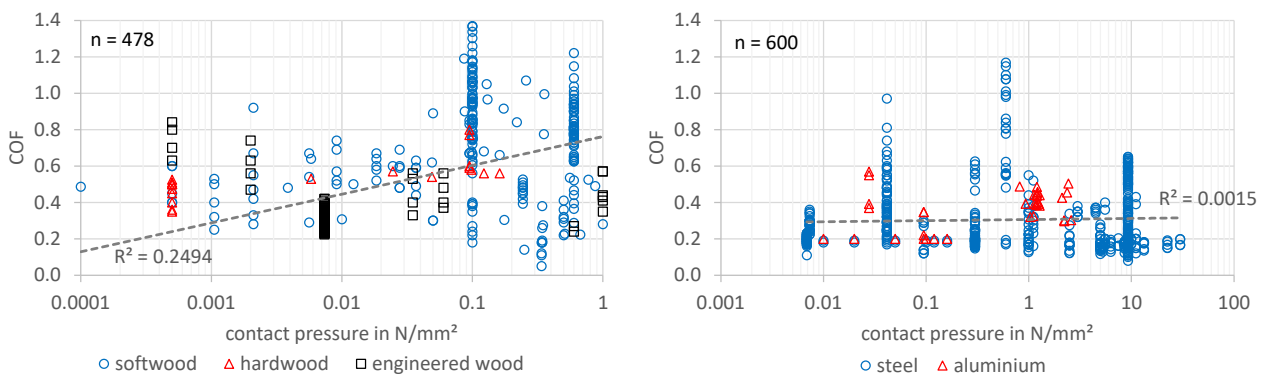


Figure 3. COF versus contact pressure for wood on wood (left) and steel on wood (right).

Table 1. Reviewed literature and respective number of friction coefficients found in the literature (this list is not intended to be exhaustive). Values of  $\mu_{stat}$  only for MC < 20%.

Publication	Total no. of tests resp. no. of series	$\mu_{stat}$	Total no. of tests resp. no. of series	$\mu_{stat}$
<b>SOFTWOOD</b>	<b>ON SOFTWOOD</b>		<b>ON STEEL / ALUMINIUM</b>	
<i>Aira et al. (2014)</i>	9	0.05-0.38	-	-
<i>Atack &amp; Tabor (1958)</i>	-	-	2	0.50-0.60 <sup>1)</sup>
<i>Blass &amp; Steige (2018)</i>	79	0.02-1.03	-	-
<i>Claus et al. (2018)</i>	19	0.14-0.89	-	-
<i>Crespo et al. (2011)</i>	10	0.39-0.53	-	-
<i>Gaber (1940)</i>	41	0.17-0.92	-	-
<i>Garcia (2012)</i>	-	-	4	0.39-0.57
<i>Gorst et al. (2003)</i>	45	0.30-0.80	159	0.30-0.70
<i>Guan et al. (1983)</i>	-	-	58	0.17-0.38
<i>Koch (2011)</i>	6	0.37-0.66	-	-
<i>Koubek &amp; Dedicova (2014)</i>	-	-	108	0.10-0.90
<i>Lemoine et al. (1970)</i>	-	-	48	0.10-0.57
<i>McKenzie &amp; Karpovich (1968)</i>	6	0.45-0.60	47	0.11-0.65
<i>Meng et al. (2008)</i>	-	-	24	0.23-0.36
<i>Möhler &amp; Herröder (1979)</i>	132	0.29-1.37	20	0.55-1.15
<i>Möhler &amp; Maier (1969)</i>	16	0.22-1.19	-	-
<i>Murase (1984)</i>	10	0.60-0.68	30	0.18-0.20
<i>Niemz &amp; Sonderegger (2017)</i>	1	0.34	-	-
<i>Park et al. (2011)</i>	20	0.44-0.74	-	-
<i>Schmidt (2018)</i>	-	-	18	0.22-0.63
<i>Seki et al. (2013)</i>	-	-	30	0.12-0.39
<i>Stošić (1959)</i>	5	0.30-0.49	-	-
<i>Xu et al. (2014)</i>	5	0.40-0.60	-	-
	sum = 404	mean = 0.48	sum = 548	mean = 0.34
<b>HARDWOOD</b>	<b>ON HARDWOOD</b>		<b>ON STEEL / ALUMINIUM</b>	
<i>Gorst et al. (2003)</i>	18	0.40-0.60	99	0.30-0.70
<i>Guan et al. (1983)</i>	-	-	14	0.20-0.30
<i>McKenzie &amp; Karpovich (1968)</i>	-	-	105	0.08-0.64
<i>Murase (1984)</i>	10	0.53-0.60	-	-
<i>Niemz &amp; Sonderegger (2017)</i>	4	0.28-0.46	-	-
<i>Stošić (1959)</i>	3	0.30-0.31	-	-
<i>Xu et al. (2014)</i>	10	0.35-0.53	-	-
	sum = 45	mean = 0.49	sum = 218	mean = 0.41
<b>ENGINEERED WOOD</b>	<b>ON SOFTWOOD / HARDWOOD</b>		<b>ON STEEL / ALUMINIUM</b>	
<i>Bejo et al. (2000)</i>	16	0.33-0.84	-	-
<i>Gorst et al. (2003)</i>	207	0.10-0.60	210	0.10-0.70
<i>Koubek &amp; Dedicova (2014)</i>	-	-	70	0.12-0.63
<i>Meng et al. (2008)</i>	192	0.23-0.42	-	-
<i>Niemz &amp; Sonderegger (2017)</i>	72	0.12-0.59	-	-
<i>Steiger et al. (2018)</i>	8	0.24-0.57	-	-
	sum = 495	mean = 0.30	sum = 280	mean = 0.25

1) MC > 20%

## 2.4 Sliding speed

The recorded sliding speeds ranged from 1-3300 mm/min for tests with wood on wood and from 1-2640000 mm/min (= 44 m/s) for tests with steel / aluminium on wood. Figure 4 shows an increase at the beginning with increasing sliding speed and later a horizontal convergence.

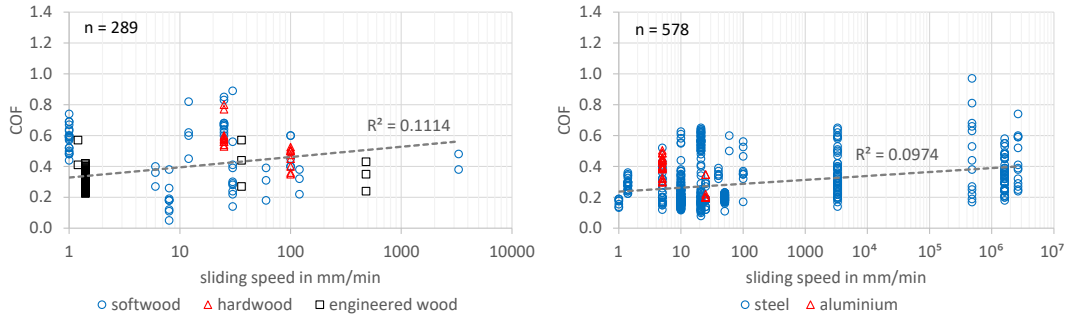


Figure 4. COF versus sliding speed for wood on wood (left) and steel on wood (right).

## 2.5 Density

Figure 5 shows no correlation between the COF and the density of the wood specimens. In general, there were very few results for tests with hardwood ( $n = 119$ ) of which for only 20 specimens the density was recorded.

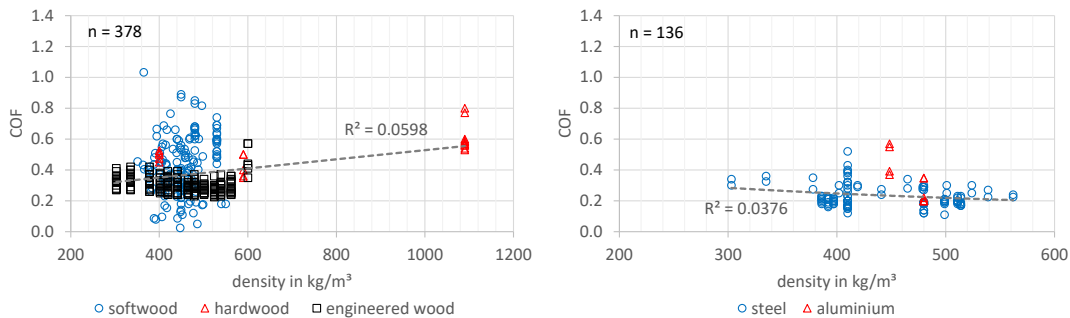


Figure 5. COF versus density for wood on wood (left) and steel on wood (right).

## 2.6 Moisture content

The moisture content was the only parameter, which was given for almost all tests. The moisture content of the wood specimens has the most distinct influence on the static COF (Figure 6). Especially for the tests with wood on wood, a moisture content greater than 20% led to a notable increase of the COF. The tests with steel / aluminium on wood were mostly independent of the moisture content of the wood.

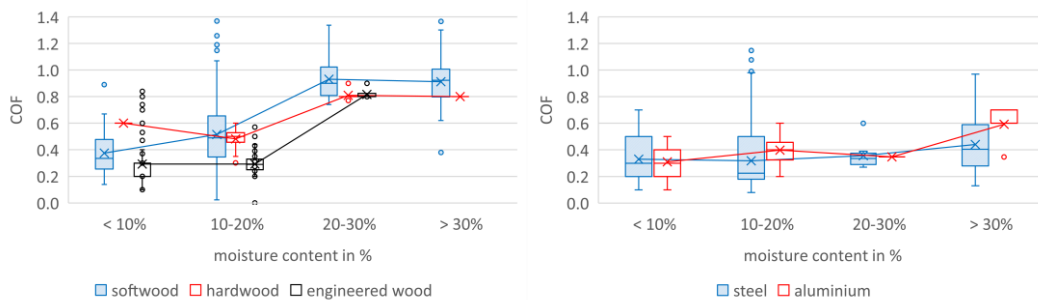


Figure 6. COF versus moisture content for wood on wood (left) and steel on wood (right).

### 2.7 Surface roughness

As expected, the surface roughness of the tested specimens had the highest influence on the COF. Figure 7 shows a box plot with three different surfaces for wood on wood (left) and four different surfaces for steel on wood (right). Treated surfaces were for example formwork panels. The classification “normal steel” was used when no other surface quality was explicitly mentioned.

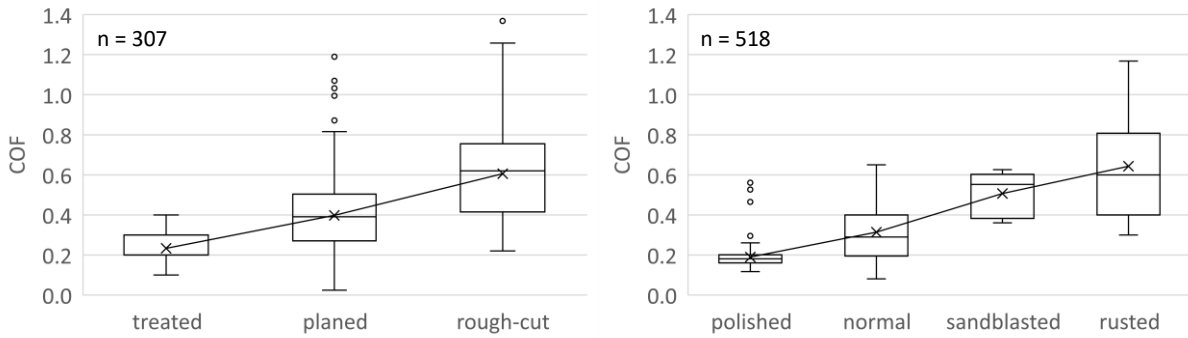


Figure 7. The effect of the surface roughness on the static COF for wood (left) and steel (right).

### 2.8 Grain direction

In many tests the orientation of the grain with regard to the sliding direction was varied, with the different orientations being parallel (grain direction of the specimens parallel to each other), perpendicular (one specimen rotated by 90°) and end grain (end grain sliding on end grain). In some publications further angles were examined, but for the sake of clarity only the three main directions parallel, perpendicular and end grain were considered in Figure 8. The difference in the COF for parallel and perpendicular was marginal, and it can be stated, that the grain direction had close to no influence on the COF. Only exception were the tests with end grain on end grain and steel on end grain, respectively.

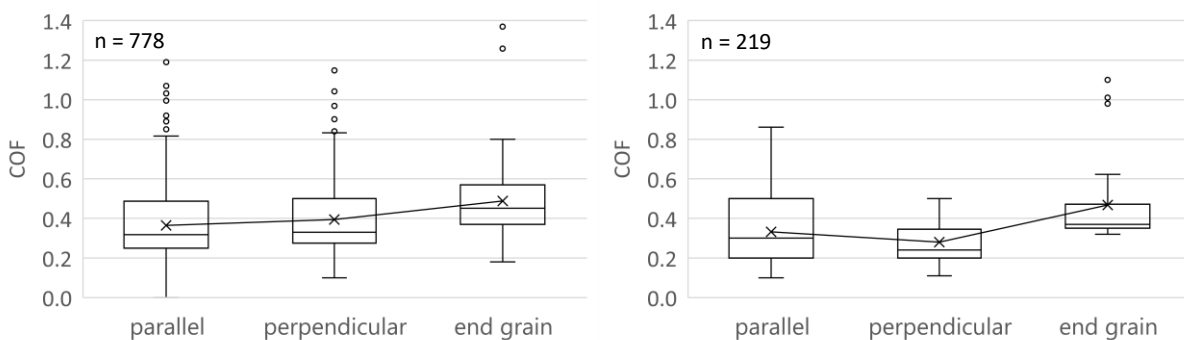


Figure 8. The effect of the grain direction of the surface on the static COF for wood on wood (left) and steel on wood (right).

### 2.9 Scatter of the COF

As it is evident by now, the values of the COF vary to a large extent for the same tested surfaces and parameters. To highlight the scatter, Figure 9 shows an exemplary plot for the COF of softwood on softwood, hardwood on hardwood, engineered wood on either softwood or hardwood, as well as steel and aluminium on softwood. The sliding

direction for all tests was parallel to the grain of the wood specimens. The moisture content was  $\leq 20\%$  and the wood surface was planed. Taking the COF for softwood as an example: the minimum is 0.02 and the maximum is 1.19, resulting in a coefficient of variation of 50%. For hardwood and aluminium the scatter is smaller, however the number of tests is equally lower.

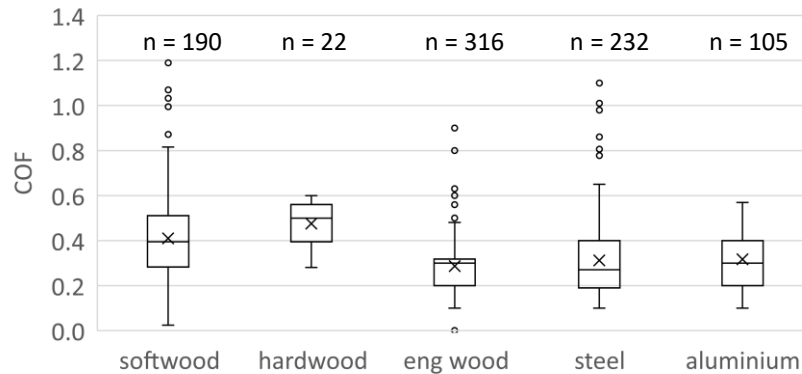


Figure 9. Scatter of the static COF (sliding direction = parallel, MC  $\leq 20\%$ , surface = planed where applicable).

### 3 Surface modification

For the connectors to reach high load-carrying capacities and stiffnesses the friction between connector and timber part should be increased. Therefore, various surface modifications have been investigated experimentally to increase the COF. In tests, the COF for each modified surface was determined and characteristic values were calculated as 5<sup>th</sup>-percentile values. As mentioned before, DVW was used for the specimens with sizes of 110 x 150 mm. The results are given in Table 2.

#### 3.1 Sanded

The top layer of the test specimen was sanded using a belt sander and sandpaper with P40 grit. The sanding was carried out perpendicular to the fibre direction of the top layer and therefore perpendicular to the sliding direction during the friction tests. A noticeable structuring was visible.

#### 3.2 Sandblasted

Each test specimen was sandblasted manually on both sides. As a result, slightly different surfaces appeared on each side and on each test specimen. During the sandblasting, it was observed that the earlywood of the veneers was removed and only the latewood remained. This resulted in a structuring along the grain direction of the cover veneers and thus parallel to sliding direction.

#### 3.3 Brushed

Both surfaces of the test specimen were brushed with a braided steel wire pot brush. A clear structuring of the surface was visible, but the roughness was hardly noticeable. In preliminary tests, only a very low COF was determined and therefore this type of surface treatment was not further pursued.

### 3.4 Coated

Two different bonding agents were used: firstly, a pasty two-component adhesive and secondly, an epoxy resin adhesive tape. The test specimens were coated either with quartz sand with a grain size of 0-2 mm or with grit with a grain size of 2-4 mm. Additionally, the specimens of one series were coated with skateboard griptape.

#### 3.4.1 Two-component adhesive (2K SE-polymer)

A two-component epoxy resin was used. The surfaces of the test specimens were sand-blasted before the adhesive was applied. A 0.5 mm thick adhesive layer was chosen for coating with quartz sand (Figure 10) and a 1.0 mm thick adhesive layer for coating with grit. The test specimens were pressed manually into the respective aggregate. The specimens cured at room temperature for one week, according to the manufacturer's instructions.



Figure 10. Coated surface with 2K epoxy resin and quartz sand 0-2 mm.

#### 3.4.2 Epoxy adhesive tape (EpoxyTape)

Epoxy resin adhesive tapes with an adhesive layer thickness of 1.0 mm and 0.1 mm were used. The tapes were applied at room temperature and then cured in the oven at a temperature of 130°C for 45 min. For both thicknesses of adhesive tape, only the quartz sand was chosen and pressed with a constant pressure of 2 N/mm<sup>2</sup> for two minutes.

#### 3.4.3 Griptape

A commercially available griptape for the top of skateboards for better grip was used. The grain of the griptape was significantly finer than that of the quartz sand and resembled sandpaper. The processing of the grip tape was significantly easier as it already combined adhesive tape and aggregate.

### 3.5 Milled

Different patterns were examined by using different milling tools on a CNC milling machine, such as a chamfer cutter for longitudinally and transversely arranged grooves or a cartridge mill for circular grooves

#### 3.5.1 Pyramid pattern

*Girardon (2014)* developed form-fitting and rigid connections with milled surfaces. Based on his studies, parallel grooves with the same depth were milled into the top layer of the test specimens using a chamfer cutter. The test specimens were then rotated by 90° and again parallel grooves were milled into the top layer resulting in small



pyramids. Test specimens with 0.5 mm, 1.0 mm, 1.5 mm and 2.0 mm deep grooves were produced. Figure 11a shows an example of a test specimen with pyramids 1.5 mm deep.

### 3.5.2 Circular grooves

Circular grooves with multiple intersections were milled 1.0 mm deep into the top layer of the DVW (Figure 11b). As a result, pyramid-like shapes remained at the edge of the test specimen while elongated grooves with a spacing of about 1.5 mm remained in the middle of the test specimen.

### 3.5.3 Scale pattern

Using a simple end mill that was inclined by 5°, longitudinal and transverse grooves were milled 1 mm deep into the surface, similar to the pyramid pattern (Figure 11c). This created a scale pattern. Again, preliminary tests resulted in a low COF and therefore this pattern was not further examined.

### 3.5.4 Embossed pattern

The pyramid pattern was milled into a steel plate. The steel plate was then pressed into the surface of the DVW. The pyramid tips penetrated about 1.0 mm into the top layer and a surface embossed with the impression of the pyramid pattern was created (Figure 11d).

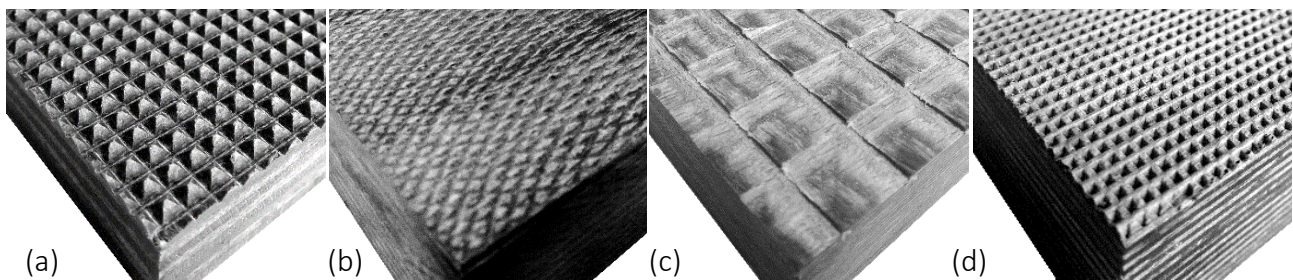


Figure 11. Milled surfaces: (a) pyramid pattern (b) circular grooves (c) scale pattern (d) embossed surface.

## 3.6 Sheet metals

Additionally to the tests with DVW and modified surfaces, some tests with different sheet metals were performed. On the one hand a chequer plate was used, which is normally applied for e.g. anti-slip flooring (Figure 12a), on the other hand sheets with perforated round holes were used. Type 1 had a clear-cut round hole (e.g. steel scaffold planks, Figure 12b) while for type 2 the excess material led to small, sharp hooks (similar to a kitchen grater, Figure 12c).

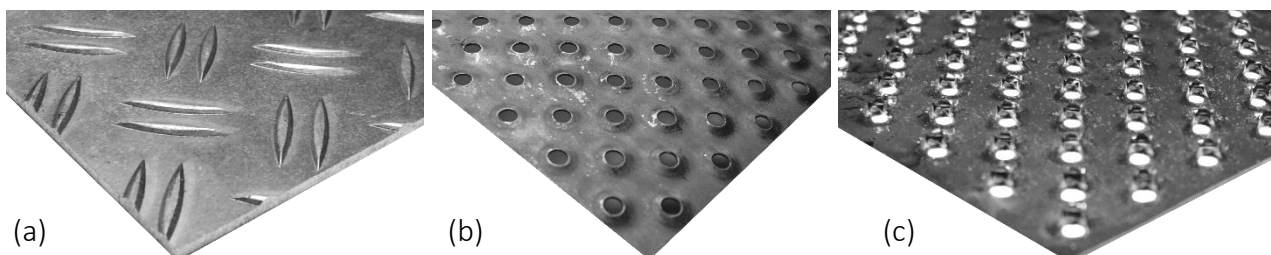


Figure 12. Sheet metals: (a) chequer plate (b) perforated sheet metal 1 (c) perforated sheet metal 2.

## 4 Tests to determine the COF

### 4.1 Test setup

The test setup is shown in Figure 13. The normal force  $F_N$  perpendicular to the friction surface was applied with a threaded rod and a spindle.  $F_N$  was measured continuously during the tests with a load cell. Spruce/fir with a mean density of  $\rho = 420 \text{ kg/m}^3$  was used for the softwood, which was stored in a standard climate 20/65 and had an average moisture content of  $u = 12\%$ . The surfaces were free of knots larger than 5 mm and without adhesive joints. The tangential force  $F$  parallel to the friction surface was applied using a universal testing machine. The entire test sequence was displacement controlled up to a displacement of 15 mm.

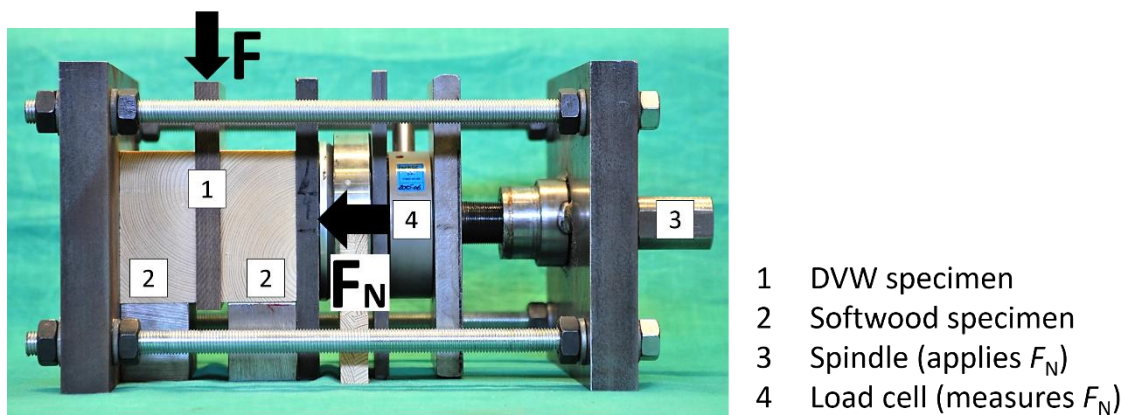


Figure 13. Test setup for friction tests.

For the tests, it was distinguished between face grain parallel and perpendicular to the sliding direction as well as end grain of the softwood. The different test configurations are highlighted in Figure 14. For the tests, side members with a similar density were chosen.

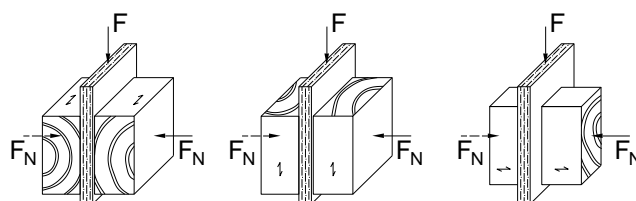


Figure 14. Grain and sliding direction.

### 4.2 Results

At the beginning, the parameters contact pressure and sliding speed were varied, in order to confirm the established trends from the literature review. The contact pressure was varied between 1, 2.5 and 6  $\text{N/mm}^2$ . The sliding speed was varied between 1, 5 and 10  $\text{mm/min}$ , to fill the gaps in the range found in the literature. No correlation between the COF and the two varied parameters was visible (Figure 15). Based on these results, the following tests were conducted with a contact pressure of 2.5  $\text{N/mm}^2$ , corresponding to the characteristic compressive strength perpendicular to

the grain of softwood. The sliding speed was set at 5 mm/min, because then a pronounced peak with the onset of sliding followed by subsequent continuous sliding was observed.

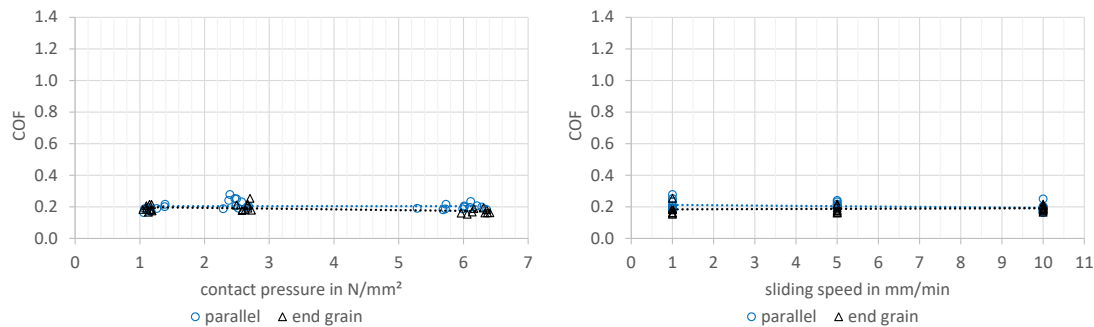


Figure 15. COF versus contact pressure (left) and sliding speed (right).

#### 4.2.1 Untreated surface, aluminium, sanded, and sandblasted surfaces

In order to create reference values and to quantify the effect of subsequent surface treatments, a first series of tests was carried out with smooth, untreated DVW. In addition, tests were performed with anodised aluminium, as found in most system connectors. On average, a COF for the smooth surface of  $\mu = 0.20$  and for aluminium of  $\mu = 0.38$  was determined. For the sanded and sandblasted surfaces the determined values were already significantly higher with  $\mu = 0.56$  and  $\mu = 0.49$ , respectively.

#### 4.2.2 Coated surfaces

For the test specimens with the two-component adhesive, adhesive failure of the coating was observed. The glue and aggregate came off the DVW almost completely. This observation was independent of the grain size of the coating (Figure 16 left). Due to the failure of the adhesive, only a lower limit for the COF was determined. This was  $\mu = 0.64$  for coating with quartz sand and  $\mu = 0.61$  for coating with grit.



Figure 16. Coated test specimens: 2K adhesive and grit (left) and griptape (right).

Adhesive failure also occurred when coating with epoxy tape with a layer thickness of 0.1 mm. However, only a few spots of the epoxy tape came off the DVW. During the tests with the epoxy tape with a thickness of 1.0 mm cohesive failure occurred and the aggregate stuck to the softwood. Overall, the results showed significantly higher friction coefficients than with the pasty epoxy resin and were on average  $\mu = 0.82$  for the thin and  $\mu = 0.74$  for the thick epoxy tape. For the tests with griptape, again no exact COF was determined due to the lack of adhesion of the griptape to the DVW (Figure 16 right). The average COF was  $\mu = 0.24$ , which is only slightly higher than for untreated DVW.

### 4.2.3 Milled surfaces

For all four examined pyramid patterns the results for the COF were significantly higher than for the surface treatments shown so far with  $\mu = 0.82$  (0.5 mm),  $\mu = 0.89$  (1.0 mm),  $\mu = 1.06$  (1.5 mm) and  $\mu = 1.15$  (2.0 mm). The larger the pyramids the deeper they pressed into the softwood and the higher the COF determined. For the tests with the circular pattern and the scale pattern, the mean values were calculated to  $\mu = 0.89$  and  $\mu = 0.66$ . The tests with the embossed pattern lead to a COF of  $\mu = 0.79$ .

### 4.2.4 Sheet metals

On average, the COF for the chequer plate was  $\mu = 0.74$  and therefore considerably higher than the COF for a normal steel or aluminium surface. The tests with the perforated sheet type 1 resulted with an even higher COF of  $\mu = 0.98$ , mainly because the surface with the small punched holes interlocked better with the softwood than the rather big texture of the chequer plate. For the tests with the perforated sheet type 2 only a lower limit of the COF was determined with  $\mu = 0.82$ . Because of the sharp hooks and the high interlocking, the tensile strength of the very thin sheets was reached.

## 4.3 Characteristic values

The characteristic values were calculated based on EN 14358. For the 5<sup>th</sup>-percentile a global coefficient of variation  $COV_g$  was calculated based on all friction tests according to EN 14545. A total of  $n = 467$  friction tests were performed and the  $COV_g$  was calculated to 0.10, resulting in  $k_s(n) = 1.76$ .

Table 2. Values for the static COF (mean and characteristic).

Surface	COF								
	face grain I			face grain II			end grain		
	mean	char.	<i>n</i>	mean	char.	<i>n</i>	mean	char.	<i>n</i>
Untreated	0.20	0.17	31	-	-	-	0.19	0.16	27
Sanded	0.56	0.47	6	-	-	-	0.47	0.40	6
Sandblasted	0.49	0.41	6	-	-	-	0.47	0.40	6
Coated with 2K-epoxy + quartz sand	0.64	0.54	3	-	-	-	0.54	0.46	3
Coated with 2K-epoxy + grit	0.61	0.52	3	-	-	-	0.69	0.58	3
Coated with EpoxyTape (0.1 mm)	0.82	0.69	3	-	-	-	0.97	0.82	3
Coated with EpoxyTape (1.0 mm)	0.74	0.63	3	-	-	-	0.82	0.69	3
Coated with Griptape	0.24	0.20	3	-	-	-	0.32	0.27	4
Milled 0.5 mm pyramid pattern	0.84	0.71	40	0.82	0.69	10	0.82	0.69	30
Milled 1.0 mm pyramid pattern	0.94	0.79	15	0.88	0.74	20	0.80	0.68	10
Milled 1.5 mm pyramid pattern	1.06	0.90	20	1.03	0.87	19	1.06	0.90	18
Milled 2.0 mm pyramid pattern	1.15	0.97	12	-	-	-	-	-	-
Milled circular grooves	0.89	0.75	14	0.78	0.66	20	0.82	0.69	13
Milled scale pattern	0.66	0.56	7	0.55	0.46	2	-	-	-
Embossed pattern	0.79	0.67	30	0.67	0.57	10	0.71	0.60	21
Aluminium	0.38	0.32	12	-	-	-	0.43	0.36	12
Chequer plate	0.74	0.63	6	0.85	0.72	6	-	-	-
Perforated sheet type 1	0.98	0.83	2	0.78	0.66	2	-	-	-
Perforated sheet type 2	0.83	0.70	3	-	-	-	-	-	-

## 5 Tests with inclined screws

### 5.1 Test setup and execution

To validate the impact of the higher COF on the load-carrying capacity, push-out tests with inclined screws were performed. Connector plates made of densified veneer wood with modified surfaces were fastened to softwood with fully threaded screws. The screws were inclined by 45°. The experimental setup is shown in Figure 17. The test specimens were loaded with a universal testing machine. The relative displacement of each connection was measured on the front and back of the test specimens. The test procedure and the evaluation were based on EN 26891. Both the ultimate test load  $F_{V,test}$  and the stiffness  $k_s$  per connector were determined. The stiffness was determined in the range between 10% and 40% of the ultimate load in the linear-elastic range.

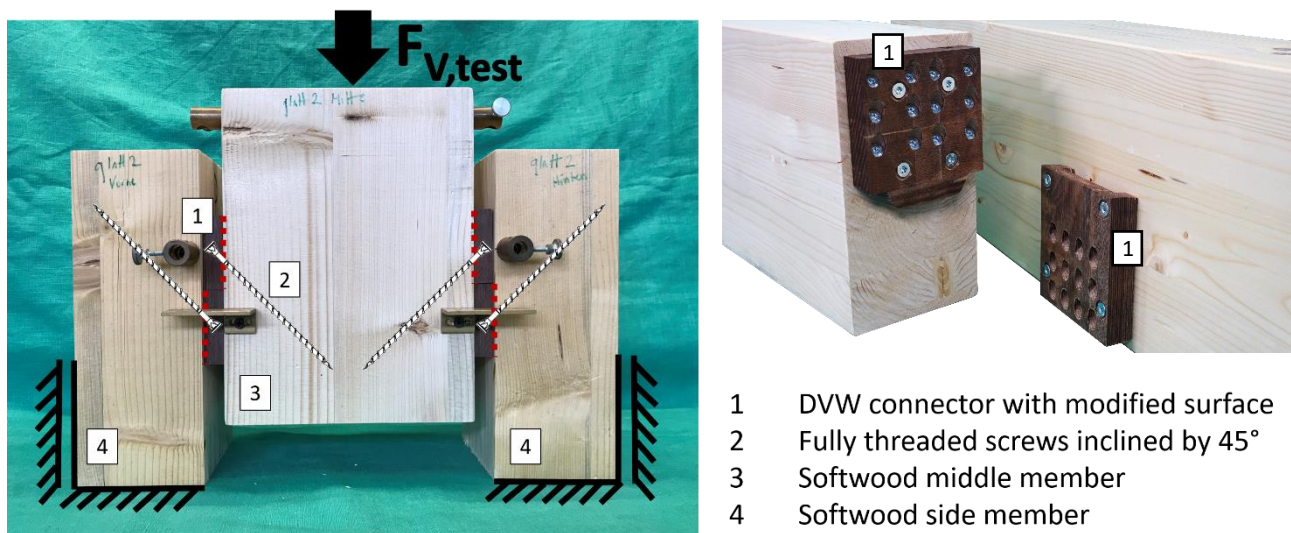


Figure 17. Test setup for push out tests with connectors with modified surfaces and inclined screws.

Table 3 summarises the tested configurations. The given number of screws is per shear plane. The series differ in the type of surface treatment, the number of screws, and the type of screws. In a first series (S1), most of the previously introduced surfaces were tested. In series 2 (S2) the screw arrangement was varied. In series 3 (S3) longer screws were used to validate the analytical model. In series 4 (S4) 15 screws were used per connector to investigate the influence of the number of screws. In series 5 (S5) the same connectors were tested with longer screws. Lastly, in series 6 (S6) and 7 (S7) two connector prototypes were tested to compare to conventional system connectors made of aluminium. For more details on the tests with the DVW connectors see *Aurand & Blass (2021)*.

### 5.2 Results

Table 3 shows the ultimate loads and corresponding stiffnesses for all surfaces examined. The ultimate loads were determined independently of the displacement. The results show a significant increase in the load-carrying capacity of the connection for any

type of surface modification. The only exception to this are the tests with griptape. The mean value of the ultimate load of the tests with untreated surface was  $F_{V,\text{test}} = 40.5$  kN per connector. Maximum loads of around 53 kN were determined for the different pyramid patterns, which implies a capacity increase of over 30% (albeit the different displacements). Load-displacement plots for all series are shown in Figure 18. Within the different series, the specimens differ in their surface treatment. For the sake of clarity, only two curves are labelled exemplarily.

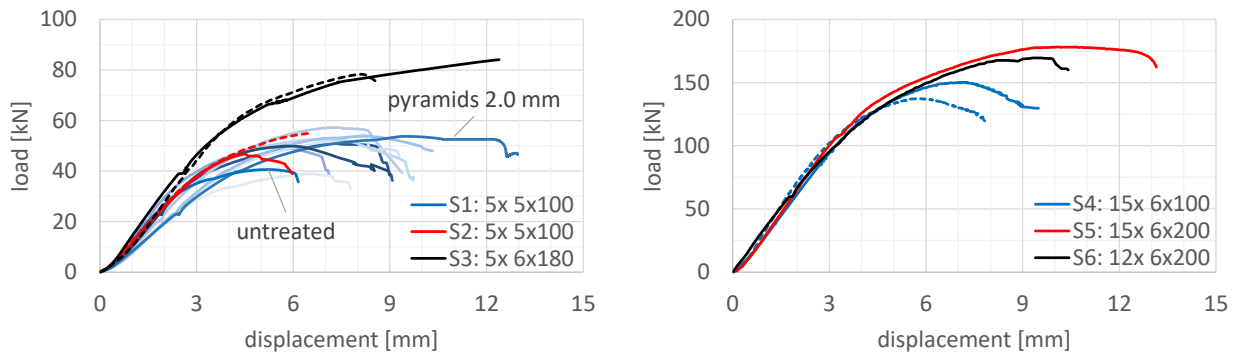


Figure 18. Load-displacement plots (averaged curves) for all tests of series 1, 2 and 3 (left) and series 4, 5 and 6 (right).

It is noteworthy that with greater pyramid size a higher COF was reached and thus a higher load-carrying capacity. However, the greater pyramid sizes led to lower stiffnesses. In general, it can be stated that higher stiffnesses were reached with less protruding surfaces (see also series 4). This might be because with the flat surfaces immediately full contact between the surfaces was reached, whereas the rougher surfaces needed some initial displacement to interlock.

The observed failure modes for series 1-4 were either a tensile failure of one or more screws in the shear plane or a withdrawal of the screws from the softwood members. For the series 5-7, with significantly higher ultimate loads, also compressive failure of the connector plates was observed. Furthermore, large displacements of the connectors were observed for these series. After opening the test specimens, clearly visible plastic hinges close to the shear plane were noticed (Figure 19). Another failure mode for series 6 and especially series 7 was compressive failure perpendicular to the grain of the timber members. Because of the large number of screws on the relatively small area, high contact pressure perpendicular to the grain occurred under the connector plates.



Figure 19. Plastic deformation of screws 6x200 (left) and 8x300 (right).

Table 3. Ultimate loads and stiffnesses and corresponding density (mean values).

	Surface	No. of tests	No. of screws	Screws [mm]	Density [kg/m <sup>3</sup> ]	$F_{V,test}$ [kN]	$k_s$ [kN/mm]
S1	Untreated	3	5	5x100	468	40.5 ± 0.8	16.7 ± 0.9
S1	Sanded	3	5	5x100	473	50.3 ± 1.6	16.3 ± 2.9
S1	Sandblasted	3	5	5x100	477	50.6 ± 1.7	17.9 ± 2.5
S1	EpoxyTape 0.1 mm + sand	3	5	5x100	465	57.8 ± 1.2	13.6 ± 0.7
S1	EpoxyTape 1.0 mm + sand	3	5	5x100	480	52.3 ± 2.3	11.4 ± 0.7
S1	Griptape	3	5	5x100	486	39.0 ± 2.1	11.4 ± 0.9
S1	Pyramid pattern 1.0 mm	3	5	5x100	440	52.9 ± 4.0	15.6 ± 0.8
S1	Pyramid pattern 1.5 mm	3	5	5x100	446	53.4 ± 1.3	12.2 ± 0.7
S1	Pyramid pattern 2.0 mm	3	5	5x100	438	52.8 ± 2.1	11.0 ± 1.0
S1	Circular grooves	3	5	5x100	477	49.9 ± 0.2	14.7 ± 1.4
S2	Pyramid pattern 1.0 mm	5	5	5x100	455	49.1 ± 3.8	14.1 ± 2.5
S2	Pyramid pattern 1.5 mm	5	5	5x100	461	47.8 ± 5.4	15.0 ± 3.2
S3	Pyramid pattern 0.5 mm	5	5	6x180	445	84.5 ± 5.3	17.8 ± 1.2
S3	Circular grooves	5	5	6x180	464	80.0 ± 2.0	17.7 ± 1.8
S4	Pyramid pattern 0.5 mm	5	15	6x100	453	153 ± 3.9	34.0 ± 3.5
S4	Embossed pattern	5	15	6x100	444	140 ± 2.9	42.6 ± 9.0
S5	Embossed pattern	3	15	6x200	429	185 ± 11	37.4 ± 3.8
S6	Pyramid pattern 0.5 mm	2	12	6x200	476	173 ± 8.5	33.3 ± 2.4
S7	Pyramid pattern 1.0 mm	3	20	8x300	440	496 ± 4.9	80.1 ± 4.3

### 5.3 Analytical model for load-carrying capacity

The analytical model to calculate the load-carrying capacity is based on equation (1). Contrary to Eurocode 5, the effective number of axially loaded screws is set to  $n_{ef} = n$ .

$$F_{V,exp} = n_{ef} \cdot F_{ax} \cdot (\cos \alpha + \mu \sin \alpha) \quad (1)$$

The withdrawal capacity  $F_{ax}$  is calculated with equation (2) given by *Blass et al. (2006)*:

$$F_{ax} = \frac{0.6 \cdot \sqrt{d} \cdot \ell_{ef}^{0.9} \cdot \rho^{0.8}}{1.2 \cdot \cos^2 \alpha + \sin^2 \alpha} \quad [N] \quad (2)$$

For the first tests with five screws  $\ell = 100$  mm (series 1 and 2) the model predicts the ultimate load quite well. The mean ratio of test load to expected load  $F_{V,test}/F_{V,exp}$  is 1.0. For the tests with 15 screws  $\ell = 100$  mm (series 4) the mean ratio is 1.1. However, for the tests with longer screws, which were designed to exceed the tensile capacity, the model's prediction of the load-carrying capacity is too high, see the blue markers in Figure 20. However, it was observed during the tests, that the test load is reached at quite large deformations. Therefore, the friction tests were re-evaluated to match the displacements in the shear plane. The adjusted COF  $\mu_{adj}$  (i.e. the COF evaluated at the same displacement as was reached in the corresponding push-out tests) is between 80 and 90% of the static COF. The expected load calculated with the adjusted COF is closer

to the test load. However, the model still overestimates the load-carrying capacity, especially for the tests with longer screw lengths (red markers in Figure 20).

On closer examination, plastic hinges in the screws were observed, due to the large deformations (see Figure 19). This led to the assumption of bending moment-normal force-shear force (MNV) interaction. To check for MNV interaction, equation (3) is appropriate, which was presented by *Blass et al. (2017)*. As long as the interaction relationship according to equation (3) is maintained, the design equations according to Eurocode 5 can be used. If the conditions are not met, the properties of the dowel-type fastener must be reduced accordingly.

$$\frac{M}{M_y} + \left( \frac{N}{f_{\text{tens}}} + \frac{V}{f_{\text{shear}}} \right)^2 = 1 \quad (3)$$

With the normal force  $N$  in the screw and the allocation of area of the screw's circular cross-section, the simultaneously acting moment  $M$  can be calculated. If these values are put into equation (3) together with the yield moment  $M_y$  and the tensile strength  $f_{\text{tens}}$ , the utilisation rates for series 6 and 7 are greater than 1.0. The shear force is here neglected: on the one hand, the screws are almost exclusively subjected to tensile load due to the inclined arrangement and on the other hand, the plastic hinges are very close to the shear plane, due to the clamping effect in the DVW. Thus, according to equation (3), it has also been analytically proven that not the entire cross-section of the screw is available for the tensile load. It is therefore suggested to reduce the tensile capacity of the screws. If the ratio of the actually existing normal force  $N$  to the maximum possible normal force  $F_{\text{tens}}$  is evaluated, a mean value of 0.9 results. The average ratio of test load to the expected load with the adjusted COF and the reduced tensile strength is  $1.04 \pm 0.1$  and the coefficient of determination has also increased significantly to  $R^2 = 0.98$  (green markers in Figure 20).

To simplify the model, the dynamic COF ( $\mu_{\text{dyn}}$ ) instead of the static COF was used in equation (1), where the dynamic COF was calculated as the ratio of the friction force during sliding to the applied normal force. The mean values for the dynamic COF for the different surfaces are distinctively smaller and were as low as 50% of its static counterparts. The mean ratio of  $F_{V,\text{test}}$  to  $F_{V,\text{exp}}$  is now significantly higher than 1.0, especially for the tests with short screws, where tensile failure was not decisive (black markers in Figure 20). Table 4 shows the progress of the mean ratio of test load to expected load for the different COF: static, adjusted and dynamic.

Table 4. Ratio of test load to expected load for different COF (mean values).

COF	Series 1	Series 2	Series 3	Series 4	Series 5	Series 6	Series 7
$\mu_{\text{stat}}$	1.02	0.87	0.91	1.05	0.97	0.76	0.91
$\mu_{\text{adj}}$	1.00	1.07	1.01	1.11	0.97	0.83	0.94
$\mu_{\text{dyn}}$	1.18	1.13	1.09	1.22	0.97	0.95	0.95
$\mu_{\text{adj}} + 0.9 \cdot f_{\text{tens}}$	1.05	1.10	1.12	1.11	0.97	0.93	0.97



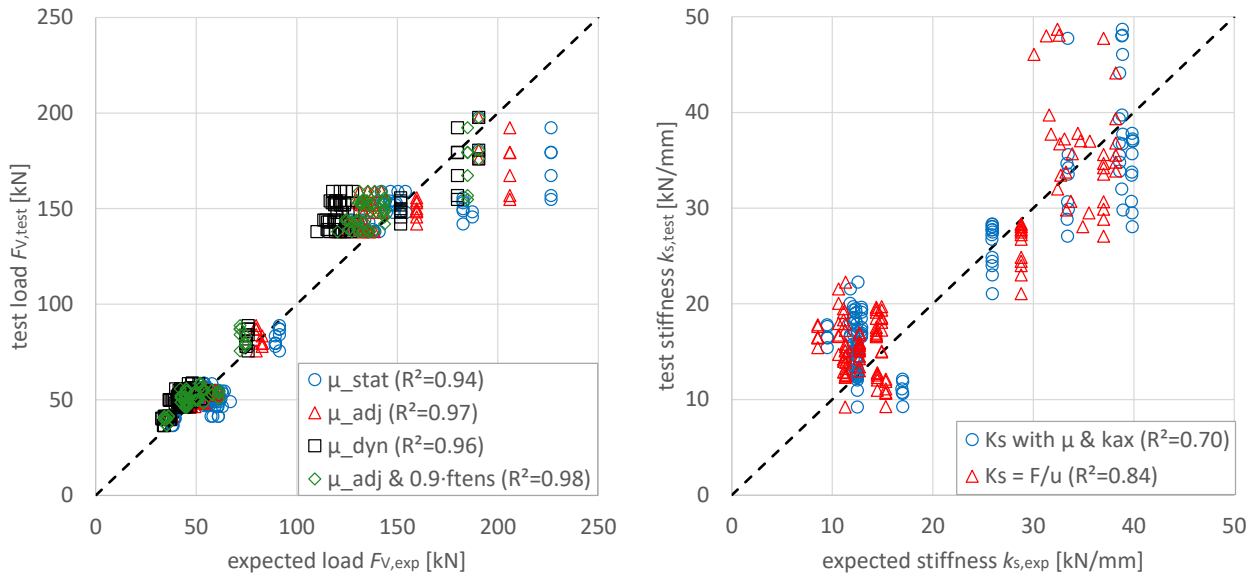


Figure 20. Test versus model for load-carrying capacity (left) and stiffness (right) of inclined screws.

Further failure modes discussed in chapter 5.2 also have to be considered, i.e. compressive failure perpendicular to the grain of the timber members as well as the load-carrying capacity of the connector itself. Thus, the capacity of the connection with inclined screws and increased shear plane friction results in the minimum of equation (4):

$$F_{V,inclined} = \min \begin{cases} n \cdot F_{ax} \cdot (\mu_{adj} \cdot \sin \alpha + \cos \alpha) \\ n \cdot 0.9 \cdot F_{tens} \cdot (\mu_{adj} \cdot \sin \alpha + \cos \alpha) \\ F_{V,connector} \\ A_{c,90,header} \cdot f_{c,90,header} \cdot k_{c,90,header} \cdot \left( \mu_{adj} + \frac{1}{\tan \alpha} \right) \end{cases} \quad (4)$$

- Where
- $n$  number of screws
  - $F_{ax}$  withdrawal capacity of the screws
  - $F_{tens}$  tensile capacity of the screws
  - $\mu_{adj}$  adjusted coefficient of friction
  - $\alpha$  angle of the inclined screws towards the connector plane
  - $F_{V,connector}$  load-carrying capacity of the connector (i.e. compressive strength depending on material)
  - $A_{c,90,header}$  effective contact area of header loaded perpendicular to grain
  - $f_{c,90,header}$  compressive strength perpendicular to grain of the header
  - $k_{c,90,header}$  coefficient for compression perpendicular to grain

## 5.4 Analytical model for stiffness

To estimate the stiffness for connections with inclined screws taking the friction into account, *Blass & Steige* (2018) derived equation (5), where  $k_{ax,1}$  and  $k_{ax,2}$  are the stiffnesses of the screw in the two connected parts, depending on the respective penetration depths.

$$K_{\text{inclined}} = n \cdot \frac{\cos^2 \alpha \cdot (1 + \mu \cdot \tan \alpha)}{\frac{1}{k_{ax,1}} + \frac{1}{k_{ax,2}}} \quad (5)$$

where  $n$  number of inclined screws  
 $k_{ax}$  axial stiffness of the screws  
 $\mu$  coefficient of friction  
 $\alpha$  angle of the inclined screws towards the shear plane

The axial stiffness can be calculated with equation (6), proposed by *Blass & Steige* (2018). The equation is derived analytically and based on 290 tests with varying parameters.

$$k_{ax} = 0.48 \cdot d^{0.4} \cdot \ell_{ef}^{0.4} \cdot \rho_m^{0.3} \quad [\text{kN/mm}] \quad (6)$$

For the two parts  $k_{ax,1}$  and  $k_{ax,2}$  of the total stiffness of the screw, different penetration lengths have to be considered. Equation (6) can be used to determine  $k_{ax,1}$ , the stiffness of the part in the softwood. However, using the same equation for calculating the axial stiffness of the part of the screw in the connector leads to too high stiffnesses and the overall stiffness of the connection  $K_{\text{inclined}}$  is overestimated. This is because the screw sits only loosely in the connector with some hole clearance. That is why it is suggested to use a calibrated value of 3.5 kN/mm for  $k_{ax,2}$ . The good fit of the model shows with the ratio of test stiffness to expected stiffness ranging from 0.65 to 1.76 and a mean value of 1.07 (blue markers in Figure 20). Alternatively, and analogous to ETAs for system connectors, the stiffness can be calculated by dividing the estimated load-carrying capacity by a fixed displacement  $u$ . For the tests with screws  $\ell = 100$  mm a displacement of  $u = 4$  mm is suitable, while for the tests with screws  $\ell > 100$  mm a displacement of  $u = 5$  mm is suitable (red markers in Figure 20). The ratio ranges here from 0.72 to 1.95 with a mean value of 1.17.

## 6 Conclusions, relation to EC 5 and outlook

The following conclusions can be drawn from the study:

- The scatter of experimentally determined friction coefficients for wood on wood is rather high, independent of the test setup and the chosen parameters.
- Based on a mean COF of 0.48 for softwood on softwood from the literature, the value of a characteristic  $\mu = 0.25$  as given in Eurocode 5 seems quite reasonable.

- The tests to determine the COF of the different surfaces showed that higher than usual COF can be obtained with easy to accomplish surface treatments. All examined surfaces led to higher COF than aluminium, which is mostly used for system connectors (only exception being the tests with griptape).
- In case coating as surface treatment is applied, the optimal solution would be a thin adhesive layer for better bonding and a small grain size for high COF
- The tests with the milled pyramid pattern showed high static COF for larger pyramids and high stiffnesses for smaller pyramids. Therefore, if a high stiffness is needed, small protruding surfaces should be chosen. And if a high load-carrying capacity is needed, surfaces with larger protruding surfaces should be chosen.
- The tests with the sheet metals showed significantly higher COF than tests with normal steel (see literature review). This shows the potential for such surface treatments for all kinds of connectors made of steel/metal, e.g. joist hangers, angle brackets, hold-downs, etc.
- The tests with inclined screws and simple connectors proved the applicability of the examined surfaces in an assembly situation. An effective interaction of treated surface and inclined screws could be established.
- The push-out tests furthermore revealed additional failure modes which should be considered for connections with inclined screws: (i) a reduction of the tensile capacity of the screws due to bending moment-normal force interaction and (ii) compressive failure perpendicular to the grain of the timber parts underneath the connector plate.

The load-carrying capacity for connections with inclined screws ( $45^\circ$ ) and a COF of  $\mu = 0.25$  as given in Eurocode 5 results in  $F_V = 1.25 \cdot F_{ax} / \sqrt{2}$ , according to equation (1). If a milled surface with a pyramid pattern with a characteristic COF of  $\mu_{stat} = 0.79$  is chosen, the load-carrying capacity for the same connection is more than 40% higher. Conversely, this also means, that fewer fasteners are needed in order to reach the same load-carrying capacity as before.

As mentioned before, series 6 and 7 were tests with prototype connectors. A comparison of the characteristic load-carrying capacity of currently available system connectors, with similar dimensions as the specimens in series 6 and 7, shows a significant increase in load-carrying capacity for connectors with treated surface and inclined screws. This is confirmed to a great extent by the ultimate load per screw (see Table 5).

To further simplify the evaluation of the COF it should be considered to use either the static or dynamic COF, instead of the adjusted COF. Because of the much lower dynamic COF, a reduction of the tensile strength of the screws would no longer be necessary. With a mean ratio of test load to expected load of 1.15 the correlation between tests and model is quite good ( $R^2 = 0.96$ ). However, for all cases where the tensile capacity is not decisive, the use of the dynamic COF would largely underestimate the load-carrying capacity. Alternatively, if the static COF is used in the model, the tensile

strength of the screws should be reduced to 75%, for an adequate fit of the model. Here the mean ratio of test to model is 1.16 and the coefficient of determination  $R^2 = 0.98$ . However, now the model would overestimate the cases with short screws, where the withdrawal capacity is decisive.

*Table 5. Comparison of characteristic load-carrying capacities and customary system connectors.*

Connector	Width [mm]	Height [mm]	Depth [mm]	Screw type [mm]	No. of screws	$F_{v,k}^{1)}$ [kN]	Load per screw [kN]
Series 6	110	220	25	6x200	24	154 <sup>2)</sup>	6.4
Pitzl HVP 88425	120	250	15+15	8x200	20	93.3	4.7
Sherpa XL 55	140	250	16+16	8x200	18	81.9	4.6
Series 7	140	558	50	8x300	40	330 <sup>2)</sup>	8.3
Pitzl HVP 88555	140	550	15+15	8x300	56	395	7.1
Sherpa XXL 280	140	570	16+16	8x200 <sup>3)</sup>	54	349	6.5

1) for glulam GL 24h

2) 5<sup>th</sup>-percentile according to EN 14358 with  $k_s(n) = 2.1$

3) max. allowed screw length according to ETA-12/0067

## 7 References

- Aira JR, Arriaga F, Íñiguez-González G, Crespo J (2014) Static and kinetic friction coefficients of Scots pine (*Pinus sylvestris* L.), parallel and perpendicular to grain direction. In: *Materiales de Construcción* 64 (315).
- Atack D, Tabor D (1958) The friction of wood. In: *Proceedings of the Royal Society of London. Series A. Mathematical and Physical Sciences* 246 (1247), S. 539–555.
- Aurand S, Blass HJ (2021) Verbinder aus Kunstharzpressholz – Versuche mit ersten Prototypen für Traglasten bis 500 kN. In: *Bautechnik* 98 (S1), S. 40–50.
- Bejo L, Lang EM, Fodor T (2000) Friction coefficients of wood-based structural composites. In: *Forest products journal* 50 (3), S. 39–43.
- Bejtka I, Blass HJ (2002) Joints with Inclined Screws. Paper 35-7-4. CIB W18 - Meeting 35. Kyoto, Japan, 2002.
- Blass HJ, Bejtka I and Uibel T (2006) Tragfähigkeit von Verbindungen mit selbstbohrenden Holzschrauben mit Vollgewinde. *Karlsruher Berichte zum Ingenieurholzbau*, Bd. 4. Universitätsverlag Karlsruhe.
- Blass HJ, Sandhaas C, Meyer N (2017) Steel-to-timber connections: Failure of laterally loaded dowel-type fasteners. Paper 50-7-1. In: *Proceedings of the INTER Meeting* 50, 28.-31. Aug. 2017. Kyoto, Japan.
- Blass HJ and Steige Y (2018) Steifigkeit axial beanspruchter Vollgewindeschrauben. *Karlsruher Berichte zum Ingenieurholzbau*, Bd. 34. KIT Scientific Publishing. Karlsruhe.
- Claus T, Seim W, Liese J (2018) Friction under cyclic loading. *World Conference on Timber Engineering WCTE*. Seoul, Korea, 2018.
- Crespo J, Regueira R, Soilán A, Díez MR, Guaita M (2011) Desarrollo de metodología para la determinación de los coeficientes de fricción estático y dinámico de diferentes especies de madera. *CIMAD 11 – 1º Congresso Ibero-LatinoAmericano da Madeira na Construção*. Coimbra, Portugal, 6/7/2011.
- Gaber E (1940) Versuche über die Reibung von Nadelholz. In: *Holz als Roh- und Werkstoff* 3 (4), S. 119–122.
- Garcia A (2012) Untersuchungen zum Tragverhalten von beschichteten HVP-Verbindern. Bachelorarbeit. *Karlsruher Institut für Technologie (KIT) - Holzbau und Baukonstruktionen* (Unveröffentlicht).
- Girardon S (2014) Amélioration des performances mécaniques des assemblages bois sur bois vissés par préparation des interfaces: Application à la réalisation d'éléments de structure. *Dissertation*. Université de Lorraine - École Doctorale RP2E.
- Gorst N, Williamson SJ, Pallett PF, Clark LA (2003) Friction in temporary works: Research report 071. Hg. v. University of Birmingham.
- Guan N, Thunell B, Lyth K (1983) On the Friction Between Steel and Some Common Swedish Wood Species. In: *Holz als Roh- und Werkstoff* 41 (2), S. 55–60.
- Koch H (2011) Untersuchungen zum Last-Verformungsverhalten historischer Holztragwerke - Der abgestirnte Zapfen. *Schriftenreihe Bauwerkserhaltung und Holzbau*, Bd. 5. Kassel Univ. Press. Kassel.

- Koubek R, Dedicova K (2014) Friction of wood on steel. Master's Thesis. Linnaeus University - Faculty of Technology.
- Lemoine TJ, McMillin CW, Manwiller FG (1970) Wood Variables Affecting the Friction Coefficient of Spruce Pine on Steel. In: *Wood Science* 2 (3), S. 144–148.
- McKenzie WM, Karpovich H (1968) The Frictional Behaviour of Wood. In: *Wood Science and Technology* 2 (2), S. 139–152.
- Meng Q, Hirai T, Koizumi A (2008) Frictional Coefficients between Timber and Some Structural Sheet Materials. In: *Journal of the Japan Wood Research Society* 54 (5), S. 281–288.
- Möhler K, Herröder W (1979) Obere und untere Reibbeiwerte von sägerauhem Fichtenholz. In: *Holz als Roh- und Werkstoff* 37 (1), S. 27–32.
- Möhler K, Maier G (1969) Der Reibbeiwert bei Fichtenholz im Hinblick auf die Wirksamkeit reibschlüssiger Holzverbindungen. In: *Holz als Roh- und Werkstoff* 27 (8), S. 303–307.
- Murase Y (1984) Friction of Wood Sliding on Various Materials. In: *Journal of the Faculty of Agriculture, Kyushu University* 28 (4), S. 147–160.
- Niemz P and Sonderegger W (2017) *Holzphysik: Physik des Holzes und der Holzwerkstoffe*. Carl Hanser Verlag. München.
- Park C-Y, Kim C-K, Kim H-K, Lee J-J (2011) Evaluation of Friction Properties According to Normal Force and Direction of Wood Grain in Real Contact Area. In: *Journal of the Korean Wood Science and Technology* 39 (5), S. 437–443.
- Popov VL (2015) *Kontaktmechanik und Reibung: Von der Nanotribologie bis zur Erdbebendynamik*:3. Aufl. Springer Vieweg. Berlin, Heidelberg.
- Schmidt T (2018) *Kontaktverbindungen für aussteifende Scheiben aus Brettsperrholz*. Karlsruher Berichte zum Ingenieurholzbau, Bd. 33. KIT Scientific Publishing.
- Seki M, Sugimoto H, Miki T, Kanayama K, Furuta Y (2013) Wood friction characteristics during exposure to high pressure: influence of wood/metal tool surface finishing conditions. In: *Journal of Wood Science* 59 (1), S. 10–16.
- Steiger R, Fink G, Nerbano S, Hack E, Beyer K (2018) Experimental investigation of friction stresses between adjacent panels made of Oriented Strand Board (OSB) and between OSB panels and glued laminated timber (GLT) frame members. In: *Materials and Structures* 51 (1), S. 123.
- Stošić DZ (1959) Untersuchungen über den statischen Reibungskoeffizienten des Holzes. In: *Holz als Roh- und Werkstoff* 17 (3), S. 86–87.
- Xu M, Li L, Wang M, Luo B (2014) Effects of Surface Roughness and Wood Grain on the Friction Coefficient of Wooden Materials for Wood–Wood Frictional Pair. In: *Tribology Transactions* 57 (5), S. 871–878.
- EN 14358:2016 Timber structures - Calculation and verification of characteristic values.
- EN 14545:2008 Timber structures - Connectors - Requirements.
- EN 26891:1991 Timber structures; Joints made with mechanical fasteners; General principle for the determination of strength and deformation characteristics (ISO 6891:1983).